

Article

The Role of Chirality and Helicity between D- and L-Valine Optical Lattices

Jingjing Li ¹, Wenqing Wang ^{2,*} and Yan Gong ^{1,2,*}

¹ School of Material Science & Engineering, Beijing Institute of Fashion Technology, Beijing 100029, China; ljj_bift215@163.com

² Department of Applied Chemistry, Beijing National Laboratory for Molecular Sciences, College of Chemistry and Molecular Engineering, Peking University, Beijing 100871, China

* Correspondence: wangwqchem@pku.edu.cn (W.W.); clygy@bift.edu.cn (Y.G.)

Received: 23 June 2018; Accepted: 3 July 2018; Published: 5 July 2018



Abstract: With the aim to investigate the role of chirality and helicity between D- and L-valine crystal lattices under Debye temperature 2–20 K, magnetic field dependence of zero-field and 1, 3 and 5 Tesla on the heat capacity were measured. The heat capacities of D- and L-valine crystals were plotted as C_p vs. T , C_p vs. $\ln T$, C_p/T^3 vs. T in the measured temperature. The four C_p/T^3 vs. T curves show a split between D- and L-valine from 2 K to 12 K ($T \ll \Theta_D$) which is due to the strength of magnetic fields. It is absent from 12 K to 20 K, which indicates the Schottky anomaly. The Bose–Einstein peak of the ($e-p$) condensation temperature is 11.20, 11.32, 11.44, 11.46 K for D-valine, and 11.49, 11.59, 11.73, 11.70 K for L-valine, respectively. This finding leads to a zero-field splitting of a broad maximum associated with the Schottky anomaly below the temperature of 12 K which is demonstrated by ($e-p$) Bose–Einstein condensation through the hydrogen of peptide bond in the alpha helix at zero momentum space onto D- and L-valine optical lattices.

Keywords: D- and L-valine optical lattices; heat capacity; temperature 2 K–20 K ($T \ll \Theta_D$); magnetic field dependence (0; 1; 3; 5 Tesla); chirality and helicity; hydrogen ($e-p$) in the alpha-helix; bose-einstein condensation; zero-momentum space

1. Introduction

Homochirality is the almost exclusive one-handedness of the chiral molecules found in living systems, e.g., L-amino acids. Its details is one of the open problems which links fundamental physics with the role of chirality and helicity. On its account, Peter W Higgs [1] and Francois Englert [2] were awarded the 2013 Nobel Prize in physics for the theoretical discovery of a mechanism that contributes to our understanding of mass of subatomic particles, broken symmetries and the mass of gauge bosons. The discovery of the mechanism for the electroweak symmetry breaking is a major goal of physics.

The roles of chirality and helicity in are emphasized by Salam [3–5]—in particular that almost all amino acids utilized in living systems are of the L-type. Starting from Z^0 interaction and Bardeen–Cooper–Schrieffer (BCS) theory, Salam [3] speculated that chirality among the twenty amino acids which make up proteins may be the analogy of “superfluidity” in superconductors.

According to Salam’s prediction, the analogy of the “superfluidity” exhibited by amino acids is to “superperfluidity in superconductors” and not to the liquid helium [4]. The difference between superconductivity and Bose superfluidity of He^4 lies in the fact that the Cooper pairs (which are bosons) are rather large objects (10^{-4} cm) compared with the interparticle distance (10^{-6} cm). An explanation in terms of quantum mechanical cooperative and condensation phenomena of ($e-n$) condensate where the ($e-n$) system has the same status as Cooper pairing [3]. The state of a given amino acid is composite of ($e-p$) system. We invent a model of ($e-p$) Bose–Einstein condensation through the hydrogen in the

helix under 2 K to 12 K ($T \ll \Theta_D$, Debye temperature). The peptide bond which give rise to protein is formed and the lattice structure is reduced to the simple form (Figure 1). The carbonyl oxygen of the i -th residue is hydrogen bonded to the H-N bond four residues along ($i + 4$).

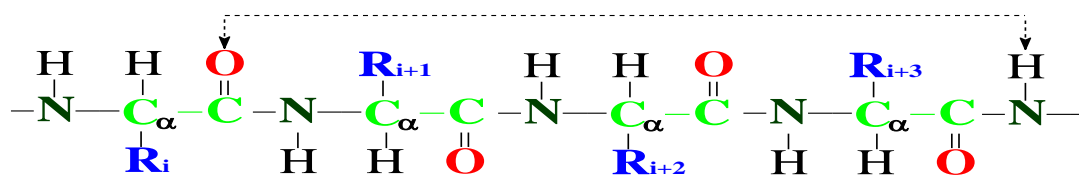


Figure 1. Spin helicity through the hydrogen of peptide bond.

In the alpha-helix, there are 3.6 amino acid residues per turn with 13 atoms along the peptide backbone per turn. This standard helical conformation is called a 3.6_{13} helix (Figure 2). The “rise” of helix is 1.5 angstroms per residue. The pitch of a standard helix is 5.4 angstroms. Ignoring side chains, the helix is about 6 angstroms in diameter.

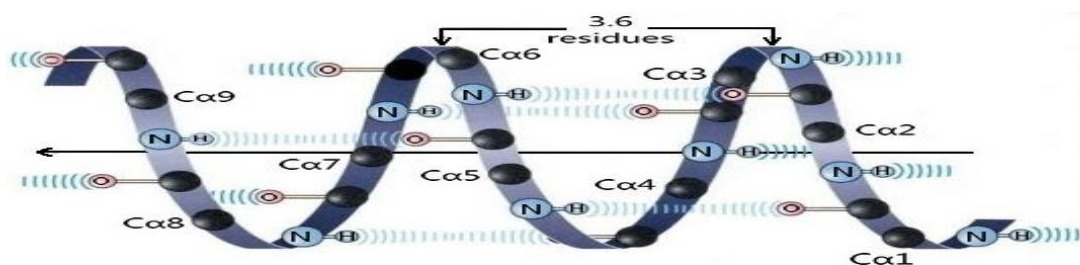


Figure 2. The standard helical conformation of 3.6_{13} helix.

This article is aimed to study the external magnetic field (0, 1, 3, 5 Tesla) dependence on the heat capacity of D- and L-valine crystal optical lattices under ultra-low temperature ($T \ll \Theta_D$). Since the electron (e) and proton (p) are fermions (not bosons), based on the Heisenberg Uncertainty Principle [6], we select the temperature from zero-point energy 2 K [7] to 20 K to search for the mechanism of (e - p) Bose–Einstein condensation at zero momentum space through the hydrogen of peptide bond in the alpha helix onto D- and L-valine optical lattices.

In fermionic superconductivity and superfluidity, a central concept is electron Cooper pairing. Our experimental measurement [8] of heat capacity of D-, L-valine crystals from 293 K, 270 K, 223 K and 173 K and optical rotatory angle study from 240 K, 250 K, 260 K, 270 K, 280 K to 290 K proved the electronic Cooper pairing and exhibited the spin superfluidity upon the transition temperature of 270 K to the superconducting state.

2. Experimental

2.1. Sample Recrystallization

The polycrystalline powders of D- and L-valine (Sigma Chemical Co., St. Louis, MO, USA, 98%) were thrice recrystallized from sterilization aqueous solution at 277 K by slow evaporation for 3 weeks, producing thin flakes elongated along the b axis with well-developed on {001} faces, washed with dropping absolute alcohol, evacuated and kept in a desiccator. The crystal purities of D- and L-valine were identified by the following procedure. The positive-ion electrospray mass spectra (EI-MS) were recorded using a Bruker APEX IV 7.0 T Fourier transform ion cyclotron resonance (FT-ICR) mass spectrometer (Bruker Daltonics, Billerica, MA, USA) equipped with an external ESI source (Analytica, Branford Inc., Branford, CT, USA) with detection limits 2 fmol for organic impurities. The purities of D- and L-valine single crystals were identified by gas chromatography mass spectrometry (GC-MS) of their N-trifluoroacetyl (TFA) isopropyl esters on Chirasil–Val capillary columns [9].

2.2. Optical Rotatory Angles of D- and L-Valine Crystal

Chiral crystals are characterized by a natural optical activity. The difficulty of the experiment was in how to measure the optical rotatory angles of monoclinic crystals of D- and L-valine, to eliminate the effect of ellipticity induced by the crystal anisotropy [10]. We measured the optical rotatory angle in biaxial crystals of monoclinic valine by projecting He-Ne laser light along its optic axes (*b* axis). The other two principal axes of refractive index ellipsoid, *a* and *c* axes were determined with Photo Elastic Modulator system (PEM-90TM). The temperature dependence of the optical rotatory angles of D-valine and L-valine crystals have been determined from 240 K, 250 K, 260 K, 270 K, 280 K to 290 K.

2.3. Magnetic-Field Dependence of Specific Heat Measurement

The magnetic-field dependence of heat capacity of D- and L-valine crystals were measured with a Physical Properties Measurement System (Quantum Design-USA PPMS-14) using the heat pulse-relaxation method. Both crystals were dried at room temperature for three days at 1.3×10^{-2} Pa, in a system trapped with liquid nitrogen. Single crystals of D-valine (11.30 mg) and L-valine (11.33 mg) with the size of 3 mm \times 4 mm \times 0.5 mm were stuck by N-grease to the holder. After loading the system they were subjected to pumping at 1.3×10^{-3} Pa for 3 h. High-precision specific heat measurements were performed on crystals with the same warming rate (1 K/min) from 2 K to 20 K under magnetic fields (H) with $H \parallel b$ axis from 0, 1, 3 up to 5 T. Heat capacity data of D- and L-valine at low temperature are almost the same as a paper in 2013 [11].

3. Results and Discussion

3.1. Enthalpy and Entropy Changes of D- and L-Valine from 2–20 K

The heat capacities of D-, L-valine crystal are plotted as C_p vs. T and C_p vs. $\ln T$ in the measured temperature (Figure 3). At constant pressure, it is given by the following equation:

$$\Delta H \equiv H(T_2) - H(T_1) = \int_2^{20} C_p dT \quad (1)$$

$$\Delta S \equiv S(T_2) - S(T_1) = \int_2^{20} \frac{C_p}{T} dT = \int_2^{20} C_p d \ln T \quad (2)$$

Magnetic field dependence of heat capacity at 2–20 K for D- and L-valine are listed in Tables 1 and 2. Based on the data in Table 1, magnetic-field dependence of the transition enthalpy and entropy changes were calculated by the usual method of graphical integration between 2 and 20 K and are listed in Table 3. The transition enthalpy ΔH and entropy ΔS of D-valine are a little higher than that of L-valine. It seems that the ground state of L-valine is lower in energy than that of D-valine.

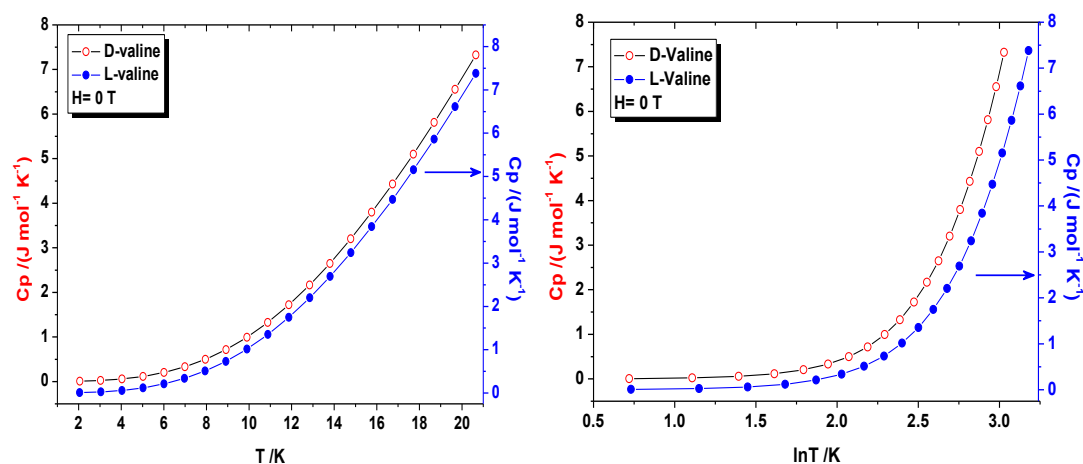


Figure 3. Low temperature C_p versus T and C_p versus $\ln T$ of D- and L-valine at zero-field.

Table 1. Magnetic-field dependence of heat capacity of D-valine (11.30 mg) at 2–20 K.

T/K	$C_p/(J \cdot mol^{-1} \cdot K^{-1})$						
H = 0 T		H = 1 T		H = 3 T		H = 5 T	
2.033	0.0072	2.029	0.00715	2.03	0.00702	2.032	0.00698
3.062	0.02587	3.061	0.02568	3.071	0.02564	3.085	0.02596
4.094	0.06483	4.097	0.06364	4.112	0.06382	4.13	0.06518
5.11	0.1304	5.115	0.1287	5.133	0.1298	5.155	0.1312
6.128	0.232	6.131	0.2301	6.151	0.2313	6.174	0.2336
7.144	0.3791	7.15	0.3778	7.165	0.3779	7.187	0.384
8.132	0.5692	8.137	0.5688	8.151	0.567	8.164	0.5708
9.146	0.8239	9.15	0.8196	9.163	0.8219	9.174	0.8215
10.119	1.125	10.125	1.124	10.14	1.124	10.151	1.126
11.113	1.491	11.119	1.491	11.133	1.491	11.14	1.492
12.122	1.927	12.123	1.928	12.137	1.928	12.145	1.933
13.135	2.425	13.134	2.425	13.146	2.426	13.152	2.431
14.14	2.974	14.142	2.981	14.147	2.979	14.156	2.982
15.205	3.612	15.154	3.579	15.175	3.592	15.156	3.582
16.166	4.234	16.174	4.243	16.171	4.242	16.178	4.245
17.218	4.97	17.207	4.964	17.199	4.958	17.195	4.957
18.165	5.691	18.168	5.681	18.174	5.677	18.175	5.68
19.197	6.452	19.194	6.454	19.192	6.454	19.184	6.45
20.183	7.256	20.192	7.255	20.19	7.253	20.193	7.27

Table 2. Magnetic-field dependence of heat capacity of L-valine (11.33 mg) at 2–20 K.

T/K	$C_p/(J \cdot mol^{-1} \cdot K^{-1})$						
H = 0 T		H = 1 T		H = 3 T		H = 5 T	
2.032	0.00694	2.027	0.00691	2.031	0.00679	2.031	0.00684
3.061	0.02477	3.062	0.02459	3.07	0.02432	3.084	0.02479
4.093	0.0619	4.099	0.06133	4.113	0.06159	4.13	0.06229
5.112	0.1244	5.118	0.1234	5.133	0.1238	5.154	0.126
6.129	0.2212	6.131	0.2195	6.152	0.2201	6.172	0.2242
7.145	0.3639	7.149	0.3624	7.165	0.3637	7.188	0.3676
8.131	0.5495	8.137	0.5476	8.15	0.548	8.166	0.5493
9.146	0.7941	9.151	0.7938	9.163	0.7932	9.175	0.7954
10.119	1.09	10.125	1.089	10.139	1.089	10.149	1.093
11.115	1.448	11.121	1.449	11.134	1.448	11.141	1.45
12.123	1.876	12.129	1.877	12.139	1.878	12.147	1.881
13.137	2.361	13.14	2.367	13.148	2.367	13.156	2.372
14.14	2.906	14.143	2.908	14.149	2.911	14.156	2.909
15.193	3.523	15.185	3.516	15.179	3.514	15.165	3.501
16.167	4.145	16.168	4.146	16.17	4.151	16.18	4.153
17.211	4.863	17.208	4.863	17.206	4.861	17.207	4.862
18.173	5.555	18.167	5.564	18.172	5.57	18.171	5.574
19.198	6.333	19.194	6.335	19.192	6.339	19.193	6.339
20.187	7.122	20.191	7.127	20.19	7.123	20.19	7.124

Table 3. Magnetic-field dependence of ΔH and ΔS in D- and L-valine crystals from 2–20 K.

H/T	Crystal	$\Delta H/(\text{J}\cdot\text{mol}^{-1})$	$\Delta S/(\text{J}\cdot\text{mol}^{-1}\cdot\text{K}^{-1})$	$\Delta H_{\text{D}}-\Delta H_{\text{L}}/(\text{J}\cdot\text{mol}^{-1})$	$\Delta S_{\text{D}}-\Delta S_{\text{L}}/(\text{J}\cdot\text{mol}^{-1}\cdot\text{K}^{-1})$
0	D-Val	39.59867	2.67648	0.9293	0.06683
	L-Val	38.66940	2.60965		
1	D-Val	39.57943	2.67387	0.90479	0.06520
	L-Val	38.67464	2.60867		
3	D-Val	39.53354	2.66950	0.87851	0.06356
	L-Val	38.65503	2.60594		
5	D-Val	39.54130	2.66987	0.89656	0.06455
	L-Val	38.64474	2.60532		

3.2. Debye Heat Capacity Anomaly and the Origin of (E-P) Bose–Einstein Condensation on D- and L-Valine Crystal Lattices

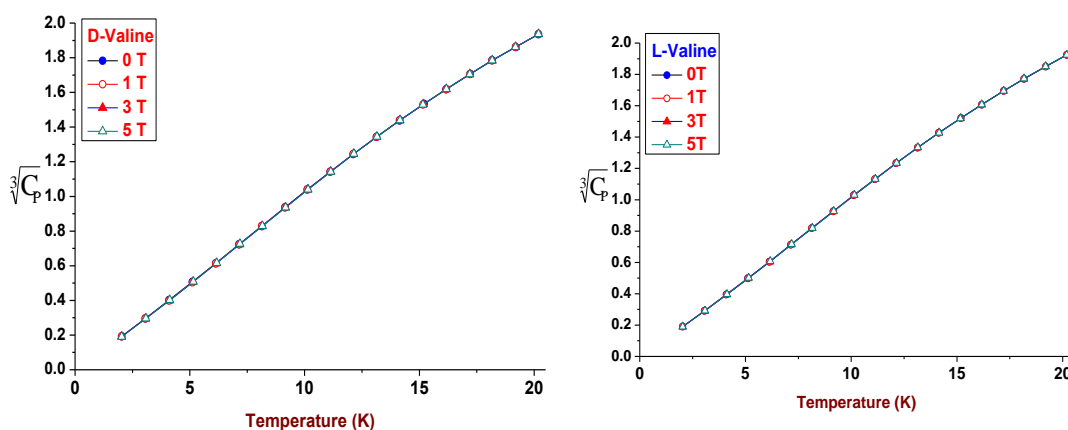
The Debye temperature Θ_{D} is an important physical parameter of crystals, which defines a division line between quantum–mechanical and classical behavior of phonons [12]. Heat capacity measurement at very low temperatures is a classical method for determining Θ_{D} [13]. At temperatures below 10 K, the Debye model predicts [14], $C_v = aT^3 = \frac{12}{5}\pi^4 R \left(\frac{T}{\Theta_{\text{D}}}\right)^3$. (C_v heat capacity at constant volume, R gas constant.). The Debye temperature follows from the following relationship under constant pressure, $\Theta_{\text{D}} = 12.480 \times \frac{T}{\sqrt[3]{C_p}}$ (Figure 4).

However, D- and L-valine crystals did not absolutely obey the Debye model at the temperature range of 2–20 K. By using a curve-fit equation from C_p/T^3 versus T plot, the Debye temperatures were calculated for the molecular crystals and the results are listed in Table 4.

By using a curve fit equation from the C_p/T^3 vs. T plot, the Debye heat capacity of D- and L-valine crystal is plotted in the measured temperature 2 K–20 K ($T \ll \Theta_{\text{D}}$), respectively (Figure 5).

Table 4. Debye temperature of D- and L-valine.

Debye Temperature (K)	H (Tesla)			
	0	1	3	5
D-valine	127.46	127.33	127.24	127.22
L-valine	128.05	127.9	127.76	127.82

**Figure 4.** $\sqrt[3]{C_p}$ versus T of D- and L-valine.

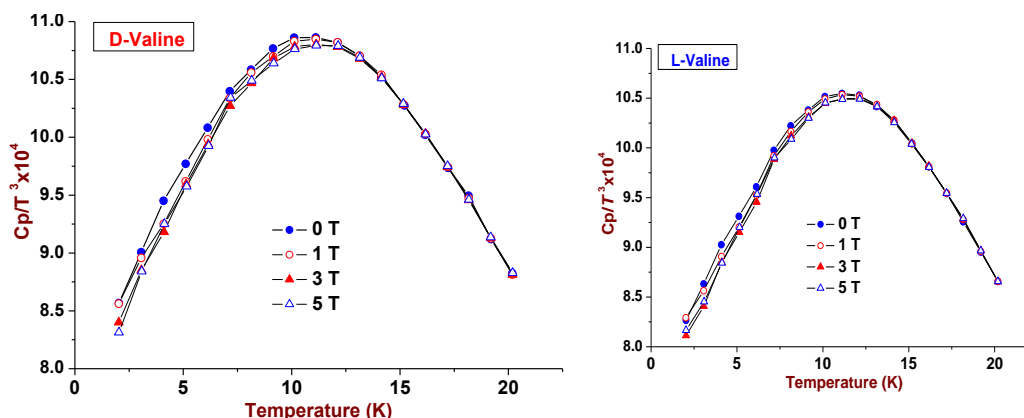


Figure 5. Temperature dependence of the heat capacities C_p/T^3 of D-, L-valine. Crystals as a function of external magnetic field with H//b axis.

Chiral D- and L-valine crystal lattices display optical activity related to the parity violation energy difference (PVED) show a dramatic change of the heat capacity with the Debye temperature leading to the appearance of a secondary maximum (developing a shoulder-type [7] structure) associated with the Schottky anomaly through the Bose–Einstein condensation temperature. Petro Barguno [15] proposed “through Bose condensation to detect PVED of chiral molecules is alternative route”. From 2 K to 20 K, most of the intramolecular motions are frozen out and the residual dynamics should be related mainly to intermolecular motions in D- and L-valine. Salam conjectured BCS superconductivity was held for the case of amino acid chains. The Cooper pairs are rather large objects (10^{-4} cm) in superconductivity transition which might occur by the hydrogen of peptide bond in helix onto the crystal lattice [11].

According to the Heisenberg Uncertainty Principle [16], 2 K is selected as the temperature of zero-point energy [17]. The necessary condition for electron–proton ($e-p$) condensation is produced by Bosonic condensates like those for Cooper pairs. The hydrogen of the peptide bond was ($e-p$) Bose–Einstein condensation at momentum space as zero momentum state from 2 K to 12 K onto D-, L-valine crystal optical lattices. The temperature of Bose–Einstein peak is 11.20, 11.32, 11.44, 11.46 K for D-valine and 11.49, 11.59, 11.73, 11.70 K for L-valine at magnetic field 0, 1, 3, 5 T, respectively (Table 5).

The overwhelmingly homochiral nature of life has left a puzzle as to whether mirror-image biological systems (Figure 6) are based on a chirally inverted version. Mirror image twins of one another have led to an intriguing question as to whether a parallel mirror image world of biology running on a chirally inverted version of molecular machinery could be found in the universe and observed in the laboratory [16].

Table 5. Temperatures of Bose–Einstein peak of D- and L-valine.

H/T	Bose–Einstein Peak (k)	
	D-Valine	L-Valine
0	11.2	11.49
1	11.32	11.59
3	11.44	11.73
5	11.46	11.7

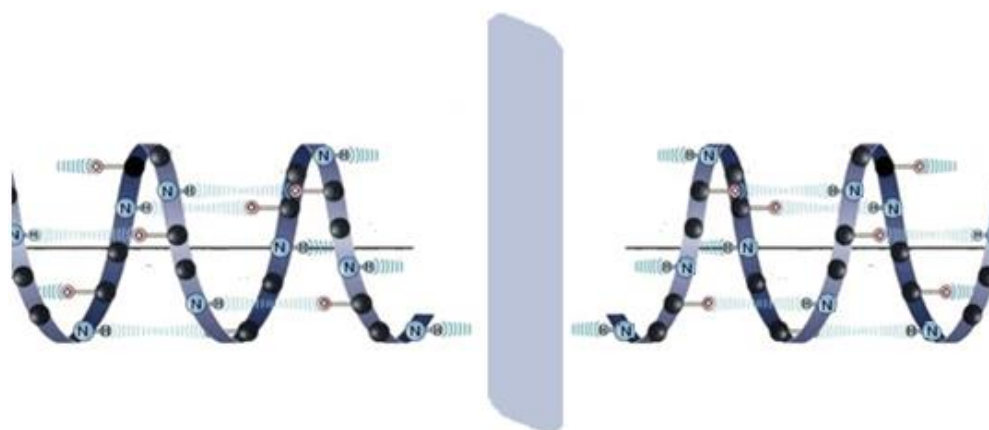


Figure 6. Natural system (left) and Mirror-image system (right).

4. Conclusions and Prospects

Our previous heat capacity experiments [8] confirmed the asymmetry of electron spin-flip transition of $N^+H \cdots O^-$ bond in D- and L-valine single crystal around 270 K. Measurement of the optical rotatory angle in polar crystals observed the slow motion of electrons at low temperature and proved the “superfluidity” of spin currents onto D- and L-valine optical lattices from 270 to 290 K.

In summary, chirality and helicity in nature has intrigued chemists and physicists for a century [17–19]. The significance of this article provides evidence for the role of chirality and helicity life. The ($e-p$) of hydrogen in peptide bond as Bose–Einstein condensation in zero momentum state from 2 K to 12 K. They are still the crystal in coordinate space. This article has not only solved the Heron Calda puzzle [20] of the condensation between electron and proton which are fermions with the constraint of equal Fermi surface. Also, a synthetic molecular system of D-valine capable of mirror-image is produced in the laboratory producing a minimal model of intrinsic chirality to study the folding behavior of helical polymers by Christian R. Boehm [21]. The fact that no known laws of physics and chemistry preclude biology’s use of either of the two chiral systems, a chirally inverted version of a molecular machinery could be reproduced in the laboratory. Furthermore, the spin-momentum coupled Bose–Einstein condensates with lattice band pseudospins [22] may provide a new platform for our study.

Author Contributions: J.L., W.W. and Y.G. conceived and designed the experiments; J.L. performed the experiments; J.L. analyzed the data; J.L. wrote the paper.

Funding: This research was supported by the National Natural Science Foundation of China (21002006, 51573211).

Conflicts of Interest: The authors declare no conflict of interest.

References

1. Higgs, P.W. Nobel Lecture: Evading the Goldstone theorem. *Rev. Mod. Phys.* **2014**, *86*, 851. [[CrossRef](#)]
2. Englert, F. Nobel Lecture: The BEH mechanism and its scalar boson. *Rev. Mod. Phys.* **2014**, *86*, 843. [[CrossRef](#)]
3. Salam, A. Chirality, phase transitions and their induction in amino acids. *Phys. Lett. B* **1992**, *288*, 153–160. [[CrossRef](#)]
4. Salam, A. The Origin of Chirality, the Role of Phase Translations and their Induction in Amino Acids. In *Chemical Evolution: Origin of Life*; Ponnampertuma, C., Chela-Flores, J., Eds.; A. Deepak Publishing: Hampton, VA, USA, 1993; pp. 101–117.
5. Salam, A. Biological Macromolecules and the Phase Transitions They Bring About. In *Conceptual Tools for Understanding Nature, Proceedings of 2nd International Symposium of Science and Epistemology Seminar, Trieste, Italy, April 1993*; Costa, G., Claucci, G., Giorgi, M., Eds.; World Scientific Publishing: Singapore, 1995; pp. 209–220.
6. Busch, P.; Heinonen, T.; Lahti, P. Heisenberg’s uncertainty principle. *Phys. Rep.* **2007**, *452*, 155–176. [[CrossRef](#)]

7. Ketterle, W. Nobel lecture: When atoms behave as waves: Bose–Einstein condensation and the atom laser. *Rev. Mod. Phys.* **2002**, *74*, 1131. [[CrossRef](#)]
8. Wang, W.Q.; Zhang, Y.F.; Gong, Y. Crystal Fine Structure and Optical Rotatory Angle Study on Spin Superfluidity of Intermolecular N+ H ... O? Hydrogen Bond Electron Cooper Pairing onto D-, L-, and DL-Valine Optical Lattices. *Acta Phys. Chim. Sin.* **2014**, *30*, 608–622.
9. Cronin, J.R.; Pizzarello, S. Enantiomeric excesses in meteoritic amino acids. *Science* **1997**, *275*, 951–955. [[CrossRef](#)] [[PubMed](#)]
10. Chen, Y.; Wang, W.Q. Temperature dependence of natural optical rotation study of D-, L-and DL-valine. *Acta Phys. Chim. Sin.* **2004**, *20*, 540–545.
11. Paukov, I.E.; Kovalevskaya, Y.A.; Boldyreva, E.V. Low-temperature thermodynamic properties of L-and DL-valines. *J. Therm. Anal. Calorim.* **2013**, *111*, 905–910. [[CrossRef](#)]
12. Jasiukiewicz, C.; Karpus, V. Debye temperature of cubic crystals. *Solid State Commun.* **2003**, *128*, 167–169. [[CrossRef](#)]
13. Pantea, C.; Stroe, I.; Ledbetter, H.; Betts, J.B.; Zhao, Y.; Daemen, L.L.; Cynn, H.; Migliori, A. Osmium’s Debye temperature. *J. Phys. Chem. Solids* **2008**, *69*, 211–213. [[CrossRef](#)]
14. Drebushchak, V.A.; Kovalevskaya, Y.A.; Paukov, I.E.; Boldyreva, E.V. Heat capacity of α -glycylglycine in a temperature range of 6 to 440 K. *J. Therm. Anal. Calorim.* **2006**, *85*, 485–490. [[CrossRef](#)]
15. Baegueno, P.; de Tudela, R.P.; Miret-Artes, S.; Gonzalo, I. An alternative route to detect parity violating energy differences through Bose–Einstein condensation of chiral molecules. *Phys. Chem. Chem. Phys.* **2011**, *13*, 806–810. [[CrossRef](#)] [[PubMed](#)]
16. Wang, Z.; Xu, W.; Liu, L.; Zhu, T.F. A synthetic molecular system capable of mirror-image genetic replication and transcription. *Nat. Chem.* **2016**, *8*, 698. [[CrossRef](#)] [[PubMed](#)]
17. Elbistan, M.; Duval, C.; Horvathy, P.A.; Zhang, P.M. Helicity of spin-extended chiral particles. *Phys. Lett. A* **2016**, *380*, 1677–1683. [[CrossRef](#)]
18. Kubota, R.; Tashiro, S.; Shionoya, M. Chiral metal-macrocycle frameworks: Supramolecular chirality induction and helicity inversion of the helical macrocyclic structures. *Chem. Sci.* **2016**, *7*, 2217–2221. [[CrossRef](#)] [[PubMed](#)]
19. Wang, Q.; Lin, S.; Qin, J.; Li, Y.; Li, B.; Yang, Y. Helical Polybissilsesquioxane Bundles Prepared Using a Self-Templating Approach. *Chirality* **2016**, *28*, 44–48. [[CrossRef](#)] [[PubMed](#)]
20. Caldas, H.; Morais, C.W.; Mota, A.L. Phase transition in asymmetrical superfluids: Equal Fermi surfaces. *Phys. Rev. D* **2005**, *72*, 045008. [[CrossRef](#)]
21. Boehm, C.R.; Terentjev, E.M. Minimal Model of Intrinsic Chirality to Study the Folding Behavior of Helical Polymers. *Macromolecules* **2014**, *47*, 6086–6094. [[CrossRef](#)]
22. Khamsehchi, M.A.; Qu, C.; Mossman, M.E.; Zhang, C.; Engels, P. Spin-momentum coupled Bose–Einstein condensates with lattice band pseudospins. *Nat. Commun.* **2016**, *7*, 10867. [[CrossRef](#)] [[PubMed](#)]

